ACTA IMEKO
ISSN: 2221-870X
June 2025, Volume 14, Number 2, 1 - 9

Phase noise contribution to the precision of differential non-linearity estimation in analog-to-digital converters using the code density test

Francisco Alegria[1]

[1] *Instituto de Telecomunicações and Instituto Superior Técnico/Universidade de Lisboa, Av. Rovisco Pais 1, 1049-001 Lisbon, Portugal*

ABSTRACT
Analog-to-digital converters, as all electronic circuits, are subject to numerous non ideal phenomena. Here we focus on the effect of phase noise on the standard deviation of the estimation of differential nonlinearity of analog to digital converters estimated using the code density test. An analytical expression is presented for the use in choosing the number of samples to use to achieve a given bound in the estimation precision or, after a test, to determine the confidence interval associated with a given estimation of differential nonlinearity. A Monte Carlo type analysis is carried out to validate the analytical expressions presented.

Section: RESEARCH PAPER

Keywords: Analog-to-digital converter; phase noise; code density test; histogram test; precision; uncertainty; sample number; Monte Carlo

Citation: F. Alegria, Phase noise contribution to the precision of differential non-linearity estimation in analog-to-digital converters using the code density test, Acta IMEKO, vol. 14 (2025) no. 2, pp. 1-9. DOI: 10.21014/actaimeko.v14i2.2087

Section Editor: Luca Callegaro, INRiM, Italy

Received March 13, 2025; **In final form** June 20, 2025; **Published** June 2025

Funding: This work was supported by FCT - Fundação para a Ciência e Tecnologia, I.P. by project reference UIDB/50008/2020, and DOI identifier 10.54499/UIDB/50008/2020.

Corresponding author: Francisco Alegria, e-mail: francisco.alegria@tecnico.ulisboa.pt

1. INTRODUCTION

Analog to-digital converters (ADCs) are fundamental in today's applications as they translate real-world signals, with the information they encode, into digital words that are easy to store and transmit due to their robustness to the presence of noise. Just to mention a few examples, we can refer to the use in telecommunications [1] where they convert voice and image into digital signals that can be transmitted over digital networks. Also, in industrial automation [2], environment monitoring [3] and automotive applications [4] they are crucial for measuring physical processes like temperature, pressure, and a myriad of other quantities from the real world.

As such, testing ADCs is essential for accessing their accuracy and performance, not only in production environment, when they leave the factory, but also during their lifetime to guarantee their reliability, longevity, and compliance with standards. The performance evaluation, which is essential in informing the ADC design [5], can be carried out using many different parameters, like signal to noise ratio, effective resolution, linearity, and dynamic range, for example. This work focuses specifically on the evaluation of differential nonlinearity (DNL) which is a metric that compares the actual code bin widths of the ADC transfer function with the ideal one [6]-[10]. There are, nonetheless, other ADC metrics that relate to linearity [11]-[13] and other parameters like gain and offset error [14] that are also important.

Determining the DNL of an ADC provides insight into accuracy and integrity of the conversion process, especially in the case of signals that do not change significantly. In high resolution medical imaging systems, poor DNL can introduce artifacts and distortions, degrading image quality and potentially leading to incorrect diagnoses or scientific observations. In digital audio processing, poor DNL can lead to quantization errors, resulting in audible artifacts such as noise or harmonic distortion in the audio signal. Just to give another example, in control systems in industrial automation and robotics that use feedback control loops, poor DNL can introduce errors in sensor readings, leading to incorrect control actions, reduced system stability, and performance.

The lack of good differential linearity often leads to a distortion in the signals converted. An instance where this is

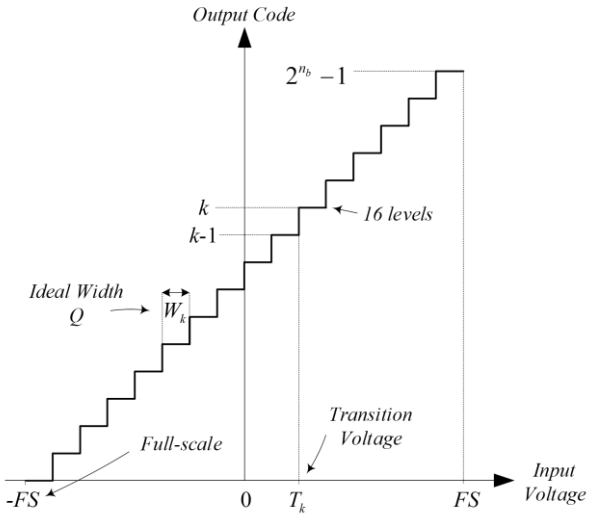

Figure 1. Example of a transfer function of an ADC with 4 bits (n_b = 4). This represents the digital output code as a function of the ADC input voltage in the range -FS to FS. The transition voltages are represented by T_k and the code bin widths by W_k. The ideal code bin width is Q.

particularly noticeable is in the conversion of audio signals where the distortion introduced by a poor differential nonlinearity can lead to unnatural or undesirable sounds. Poor DNL can cause the noise floor to modulate unpredictably with changes in signal amplitude, leading to audible artifacts such as quantization noise modulation. Accurate stereo imaging and spatial localization of sound sources depend on the left and right channels of stereo audio recording and playback systems being precisely matched. Unbalanced or distorted channels can be introduced by poor DNL, which can alter how audio sources are perceived to be wide, deep, and positioned within the stereo field. As a result, you can have a less engaging listening experience.

In image related applications, subpar DNL in ADCs can jeopardize the picture and video data's accuracy, quality, and visual integrity. Colour reproduction errors, contrast and detail loss, image processing artifacts, moiré patterns and aliasing effects, colour banding and posterization, and inaccurate motion depiction are some examples of how this can appear. These impacts have the potential to lower the overall visual quality and realism of photos and films in a variety of contexts, such as broadcasting, medical imaging, photography, videography, and surveillance. When more than one signal is present this can also contribute to intermodulation distortion.

The presence of non-ideal phenomena like additive noise [15], frequency error [16], jitter [17] and phase noise [18], [19], for example, will affect the number of counts of the histogram in a random way leading to estimation uncertainty. Of course, phase noise and jitter also affect the bias and precision of other test methods like the ones based on least squares fitting of data points [20], [21]. Even in the case of the code density test, subject of this work, other stimulus signal shapes, besides a sinewave, can be used [22]-[24].

In this work, in particular, we focus on the effect that the presence of phase noise has on the precision of DNL estimation. An analytical expression that relates the DNL estimation standard deviation, with the phase noise standard deviation and the number of samples acquired, is presented. This expression allows for an engineer to choose the proper number of samples to use, given a certain amount of phase noise present, in order to reach a desired level of precision in the estimated values of DNL. On the other hand, after the ADC test has been carried out, when specifying the estimated DNL values, it is important to add a confidence interval, that is, a numerical range of values inside which the actual value of the DNL is believed to be, with a given probability (confidence level).

2. THE CODE DENSITY TEST

Different metrics can be used to characterize the performance of an ADC. The one which is addressed in the work is the transfer function of the ADC, that is, the relation between analogue input and digital output. In Figure 1 we see an example of the transfer function for a 4-bit ADC. In practice more bits are used, which range typically from 8 to 32, but 4 is enough for illustration purposes.

In this figure the horizontal axis represents the input signal range, usually a voltage, from *-FS* to *FS* ("full-scale"). In the vertical axis we can observe the digital output codes. There are 2^{n_b} output codes in a n_b-bits ADC. They are numbered from 0 to $2^{n_b}-1$. The transfer function is thus a step-wise one since only a discrete set of output codes is possible. The transition voltage T_k represents the value of the input voltage that lies in the transition between output code $k-1$ and output code k.

A common way to characterize an ADC is to use the Code Density Test, also known as the Histogram Test. In this test method a periodic stimulus signal with frequency f is applied, usually a sinewave but other stimulus signals, like triangular or ramp waves, for example, have been used [7], [8], [25]. A given number of samples (M) are acquired at a sampling rate f_s, and the resulting digital output codes are collected and used to build a histogram where each bin has a value corresponding to the number of samples with that output code ("number of counts"). It is more common to compute the cumulative histogram which has in each bin the number of counts with a given output code or lower. These are illustrated in Figure 2.

The number of samples in each bin is then counted and used to estimate the ADC properties. The ADC transition voltages, for example, are estimated using the cumulative histogram using

$$\hat{T}_k = C - A\cdot\cos\left(\pi\frac{c_{k-1}}{M}\right),\ \ k=1,2,\ldots,2^{n_b}-1\,, \tag{1}$$

where C is the sinusoidal stimulus signal offset, A is the stimulus signal amplitude, c_k is the number of counts of bin k of the cumulative histogram and M is the total number of samples acquired. Using those voltages, we can also compute the code bin widths using

$$\widehat{W}_k = \hat{T}_{k+1} - \hat{T}_k\ \ ,\ \ k=1,2,\ldots,2^{n_b}-2\,. \tag{2}$$

Note that these widths ideally would have the value Q given by

$$Q = \frac{2\cdot FS}{2^{n_b}}. \tag{3}$$

If the ADC had an ideal behaviour, the transition voltages would be given by

$$T_k^{\text{ideal}} = -FS + Q\cdot k\,,\ \ k=1,2,\ldots,2^{n_b}-1. \tag{4}$$

If the actual transition voltages differed from the ideal ones just by a multiplicative and one additive factor so that:

$$T_k^{\text{ideal}} = G\cdot T_k + V_{os}\,,\ \ k=1,2,\ldots,2^{n_b}-1\,, \tag{5}$$

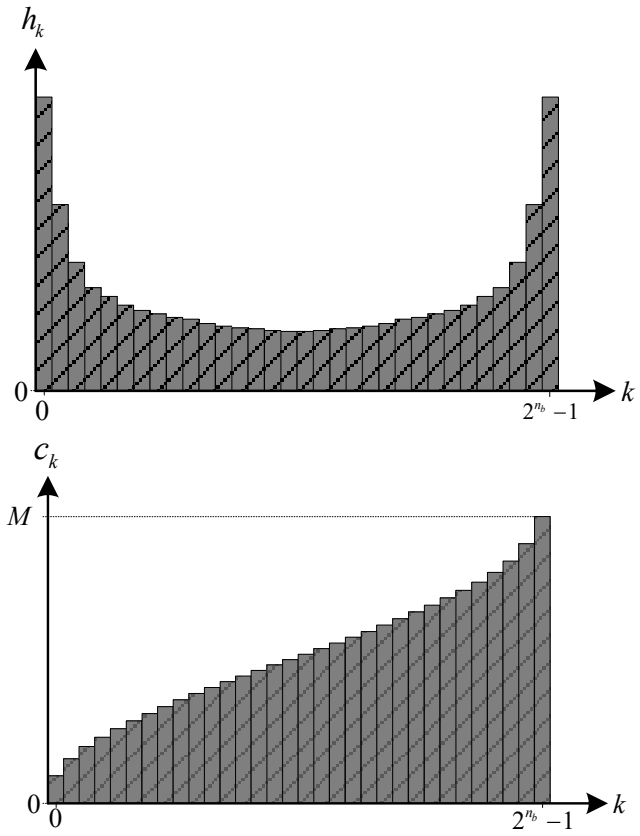

Figure 2. Histogram on the top and cumulative histogram on the bottom for the case of an ADC with 4 bits. We thus have $2^4 = 16$ bins.

then all the code bin widths would be the same, albeit with a value different from Q because of the gain G. Note that we use in the case of the transition voltages, as an example, T_k^{ideal} for the ideal value, T_k for the real value and $\hat{T}_k$ for the estimated value. The fact that in practice all the code bin widths are different from each other (and the ideal value) is what is described by the differential non-linearity parameter:

$$\widehat{DNL}_k = \frac{G \cdot \widehat{W}_k - Q}{Q} \quad , \quad k = 1, 2, \ldots, 2^{n_b} - 2 \, . \tag{6}$$

The DNL is thus estimated from the number of counts of the cumulative histogram. Because of random effects, each time a signal acquisition is made, the sample values obtained are different and so will the estimated DNL values. In this work we study their standard deviation as a function of phase noise standard deviation.

Here we consider that the randomness of the sample codes arises only due to the presence of phase noise in the stimulus signal. This noise is considered normally distributed with a variance σ_θ^2. This will lead to the estimated DNL values also being random, with a normal distribution and with a variance that we will determine next.

In the past a similar type of study has been carried out for other sources of non-ideal behaviour like additive noise [26]. Regarding the presence of phase noise, it has been shown in the past [27] that this test method is not biased by the presence of phase noise. The joint effect of the simultaneous presence of phase noise and additive noise has been considered in [28].

3. VARIANCE OF THE NUMBER OF COUNTS OF THE HISTOGRAM

The presence of phase noise in the test setup is described mathematically using variable θ in the expression the voltage of the acquired samples:

$$v_j = C + A \cdot \cos\left(2\,\pi\, f \cdot t_j + \varphi + \theta\right), \quad j = 0, 1, \ldots, M-1 \, , \tag{7}$$

where C is the offset, A is the amplitude, f is the frequency and φ is the initial phase of the sinewave in the absence of phase noise described by θ. In this case the M samples are acquired at a constant rate. In order to ease the presentation, we introduce the normalized sample voltage using:

$$y_j = \frac{v_j - C}{A} = \cos\left(2\,\pi\, f \cdot t_j + \varphi + \theta\right), \quad j = 0, 1, \ldots, M-1 \tag{8}$$

and the ideal phase of each sample (without phase noise) using:

$$\gamma_j = 2\,\pi\, f \cdot t_j + \varphi \ , \ j = 0, 1, \ldots, M-1 \, . \tag{9}$$

We can thus write the normalized sample voltage as a simple function of the normalized phase and the amount of phase noise:

$$y_j = \cos\left(\gamma_j + \theta\right) \ , \ j = 0, 1, \ldots, M-1 \, . \tag{10}$$

As mentioned before, we are considering the case of a normally distributed phase noise with a probability density function that we are going to represent by g_θ. The sample voltage, given by y_j, is thus also a random variable with probability function given by

$$g_{y_j}(y|\gamma_j) = \sum_{m=-\infty}^{\infty} \frac{g_\theta(\theta_m)}{\sqrt{1-y^2}}, \tag{11}$$

where

$$g_\theta(\theta) = \frac{1}{\sigma_\theta \cdot \sqrt{2\,\pi}} \cdot \mathrm{e}^{-\frac{\theta}{2\,\sigma_\theta^2}} \, . \tag{12}$$

Since there are two instants with the same voltage in each period of the stimulus signal, we actually have

$$g_{y_j}(y|\gamma_j) = \sum_{m=-\infty}^{\infty} \frac{g_\theta(\theta 1_m)}{|s'(\theta 1_m)|} + \frac{g_\theta(\theta 2_m)}{|s'(\theta 2_m)|}, \tag{13}$$

where s' is the stimulus signal derivative taking at the roots which are

$$\theta 1_m = \mathrm{acos}(-y) - \gamma_j + 2\,\pi\, m \tag{14}$$

and

$$\theta 2_m = -\mathrm{acos}(-y) - \gamma_j + 2\,\pi\, m \, . \tag{15}$$

Inserting them into (13), and using (12), leads to

$$g_{y_j}(y|\gamma_j) = \frac{\displaystyle\sum_{m=-\infty}^{\infty} \left[\mathrm{e}^{-\frac{\mathrm{acos}(-y)-\gamma_j+2\,\pi\, m}{2\,\sigma_\theta^2}} + \mathrm{e}^{-\frac{-\mathrm{acos}(-y)-\gamma_j+2\,\pi\, m}{2\,\sigma_\theta^2}} \right]}{\sigma_\theta\,\sqrt{2\,\pi}\,\sqrt{1-y^2}} \tag{16}$$

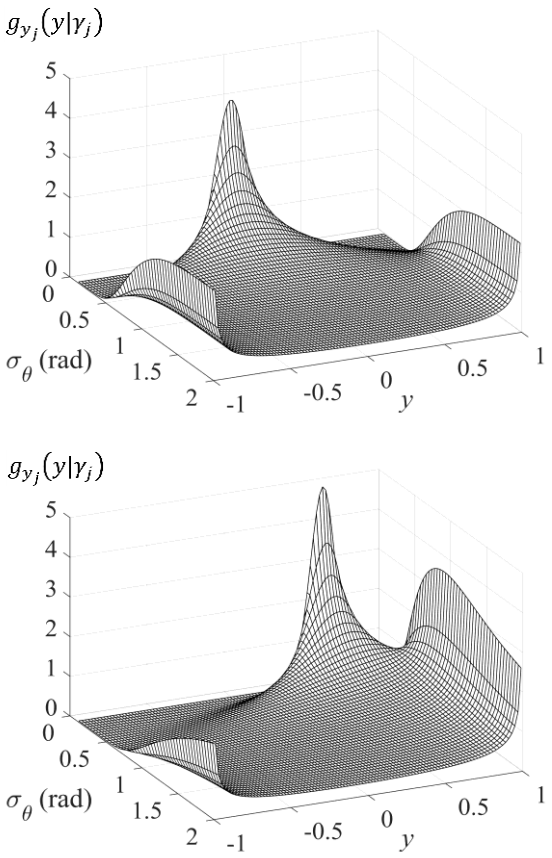

Figure 3. Probability density function for the normalized sample voltage as a function of normalized sample voltage and phase noise standard deviation for two values of ideal sample phase: $\gamma = 0.5\pi$ rad (top) and $\gamma = 0.7\pi$ rad (bottom).

for the probability density function of the normalized sample voltage. This function is represented in Figure 3 for the case of an ideal sample phase, γ_j, of $0.5\ \pi$ rad (top) and $0.7\ \pi$ rad (bottom). Note that the graph does not extend all the way up to a null phase noise standard deviation, $\sigma_\theta = 0$, because that would lead to an infinite probability density.

Note also that the location of the peak of the probability density figure observed in that figure depends on the value of the ideal phase γ_j. These two graphs are similar to the ones shown in [29] and [30]. Actually, the next two figures shown here are also similar to the ones in those works by the same author. They are included here for completeness of this presentation since the mathematical derivation carried out from the sample voltages to the variance of the number of counts of the histogram is the same.

The probability of a given sample belonging to a certain class k of the histogram, c_k, is given by

$$p_k(\gamma_j) = \int_{U[k]}^{U[k+1]} g_{y_j}(y|\gamma_j) \cdot \mathrm{d}y \tag{17}$$

where $U[k]$ and $U[k+1]$ are two consecutive normalized transition voltages.

It is thus useful, at this point, to introduce a random variable w_k, with a binomial distribution that takes the value 1 if a sample with phase γ_j belongs to class k of the histogram, and the value 0 if it does not. Its probability density function is thus given by

$$g_{w_k}(w|\gamma_j) = \begin{cases} p_k(\gamma_j) & ,\ w = 1 \\ 1 - p_k(\gamma_j) & ,\ w = 0 \end{cases} \tag{18}$$

The average value of this binomial variable is

$$\mu_{w_{k|\gamma_j}} = p_k(\gamma_j) \tag{19}$$

and its variance is

$$\sigma^2_{w_{k|\gamma_j}} = p_k(\gamma_j) \cdot [1 - p_k(\gamma_j)] \tag{20}$$

With this variable in hand, we can now proceed to compute the statistics of the number of counts of the histogram. Starting with the probability density function of c_k conditional on the ideal sample phase (sample phase without phase noise),

$$g_{h_k}(h|\phi) = g_{w_k}(w|\gamma_0) *\ldots* g_{w_k}(w|\gamma_{M-1}) \tag{21}$$

we have

$$g_{h_k}(h) = \frac{1}{2\,\pi}\int_{-\pi}^{\pi} g_{h_k}(h|\varphi) \cdot \mathrm{d}\varphi \tag{22}$$

The average value of this variable is given by

$$\mu_{h_k} = \sum_{h=0}^{M} h \cdot g_{h_k}(h) \tag{23}$$

which, after inserting (22), leads to

$$\mu_{h_k} = \sum_{h=0}^{M} h \cdot \frac{1}{2\,\pi}\int_{-\pi}^{\pi} g_{h_k}(h|\varphi) \cdot g_\varphi(\varphi) \cdot \mathrm{d}\varphi \tag{24}$$

where $g_\varphi(\varphi)$ is the probability density function of the initial phase which is considered to be uniformly distributed between 0 and 2 π:

$$g_\varphi(\varphi) = \begin{cases} \dfrac{1}{2\,\pi}\ , -\pi < \varphi < \pi \\ 0, \qquad \text{otherwise}\ . \end{cases} \tag{25}$$

Rearranging this we obtain

$$\mu_{h_k} = \frac{1}{2\,\pi}\int_{-\pi}^{\pi}\left[\sum_{h=0}^{M} h \cdot g_{h_k}(h|\varphi) \cdot g_\varphi(\varphi)\right]\mathrm{d}\varphi\ . \tag{26}$$

The term in square brackets is the average of the number of counts of the histogram, conditional on the ideal sample phase, represented here by

$$\mu_{c_h|\varphi} = \sum_{h=0}^{M} h \cdot g_{h_k}(h|\varphi) \cdot g_\varphi(\varphi)\ . \tag{27}$$

We thus have, for the average of the number of counts,

$$\mu_{h_k} = \frac{1}{2\pi}\int_{-\pi}^{\pi} \mu_{h_k|\varphi} \cdot \mathrm{d}\varphi\ . \tag{28}$$

We can now use the fact that

$$h_k = \sum_{k=0}^{M-1} w_k\ , \tag{29}$$

the conditional average of the number of counts of the histogram can be expressed through the conditional average of the variable w_k:

$$\mu_{c_k|\varphi} = \sum_{j=0}^{M-1} \mu_{w_k|\gamma_j} \,. \tag{30}$$

Inserting (9) leads to

$$\mu_{h_k} = \frac{1}{2\,\pi}\int_{-\pi}^{\pi}\left[\sum_{j=0}^{M-1} \mu_{w_k|2\,\pi\,\rho\,j+\varphi}\right]\mathrm{d}\varphi \,. \tag{31}$$

Exchanging the integral with the summation leads to

$$\mu_{h_k} = \sum_{j=0}^{M-1}\left[\frac{1}{2\,\pi}\int_{-\pi}^{\pi} \mu_{w_k|2\,\pi\,\rho\,j+\varphi}\,\mathrm{d}\varphi\right]. \tag{32}$$

Note now that the conditional average of w_k is a periodic function of the initial phase. This function has a period of 2 π. The term in the square bracket is thus the average value of that conditional average. Since all the terms in the summation are the same, we get

$$\mu_{h_k} = \frac{M}{2\,\pi}\int_{-\pi}^{\pi} \mu_{w_k|\varphi}\,\mathrm{d}\varphi \,. \tag{33}$$

Finally, making use of $\mu_{w_{k|\gamma_j}} = p_k(\gamma_j)$ leads to

$$\mu_{h_k} = \frac{M}{2\,\pi}\int_{-\pi}^{\pi} p_k(\varphi)\,\mathrm{d}\varphi \,. \tag{34}$$

Repeating now this derivation for the second raw moment of the number of counts of the cumulative histogram, we have

$$m_{2h_k} = \sum_{c=0}^{M} c^2 \cdot g_{c_k}(c) \,. \tag{35}$$

Inserting again (22) leads to

$$\begin{aligned} m_{2c_k} &= \sum_{c=0}^{M} c^2 \cdot \frac{1}{2\,\pi}\int_{-\pi}^{\pi} g_{c_k}(c|\varphi)\cdot \mathrm{d}\varphi \\ &= \frac{1}{2\,\pi}\int_{-\pi}^{\pi}\left[\sum_{c=0}^{M} c^2 g_{c_k}(c|\varphi)\right]\cdot \mathrm{d}\varphi \,. \end{aligned} \tag{36}$$

The term in the square bracket is the second raw moment conditional on the number of counts of the cumulative histogram. We can thus write

$$m_{2h_k} = \frac{1}{2\,\pi}\int_{-\pi}^{\pi} m_{2h_k|\varphi}\cdot \mathrm{d}\varphi \,. \tag{37}$$

This second raw moment can thus be written as the sum of the variance with the square of the average:

$$m_{2h_k} = \frac{1}{2\,\pi}\int_{-\pi}^{\pi} \sigma^2_{h_k|\varphi}\,\mathrm{d}\varphi + \frac{1}{2\,\pi}\int_{-\pi}^{\pi} \mu^2_{h_k|\varphi}\,\mathrm{d}\varphi \,. \tag{38}$$

Inserting now (30) and a similar expression for the variance, which is

$$\sigma^2_{h_k|\varphi} = \sum_{j=0}^{M-1} \sigma^2_{w_k|2\pi\rho j+\varphi} \,, \tag{39}$$

we get

$$\begin{aligned} m_{2h_k} &= \frac{1}{2\,\pi}\int_{-\pi}^{\pi}\left[\sum_{j=0}^{M-1} \sigma^2_{w_k|2\pi\rho j+\varphi}\right]\mathrm{d}\varphi \\ &\quad + \frac{1}{2\,\pi}\int_{-\pi}^{\pi}\left[\sum_{j=0}^{M-1} \mu_{w_k|2\pi\rho j+\varphi}\right]^2 \mathrm{d}\varphi \,. \end{aligned} \tag{40}$$

At this point it will be convenient to swap, in the first term of the right side, the integral with the summation:

$$\begin{aligned} m_{2h_k} &= \sum_{j=0}^{M-1}\left[\frac{1}{2\,\pi}\int_{-\pi}^{\pi} \sigma^2_{w_k|2\pi\rho j+\varphi}\,\mathrm{d}\varphi\right] \\ &\quad + \frac{1}{2\,\pi}\int_{-\pi}^{\pi}\left[\sum_{j=0}^{M-1} \mu_{w_k|2\pi\rho j+\varphi}\right]^2 \mathrm{d}\varphi \,. \end{aligned} \tag{41}$$

Repeating the same procedure used for the average we get

$$\begin{aligned} m_{2h_k} &= \frac{M}{2\,\pi}\int_{-\pi}^{\pi} \sigma^2_{w_k|\varphi}\,\mathrm{d}\varphi \\ &\quad + \frac{1}{2\,\pi}\int_{-\pi}^{\pi}\left[\sum_{j=0}^{M-1} \mu_{w_k|2\pi\rho j+\varphi}\right]^2 \mathrm{d}\varphi \,. \end{aligned} \tag{42}$$

We can now insert (19) and (20) to obtain

$$\begin{aligned} m_{2h_k} &= \frac{M}{2\,\pi}\int_{-\pi}^{\pi} p_k(\varphi)\,\mathrm{d}\varphi - \frac{M}{2\,\pi}\int_{-\pi}^{\pi} p_k^2(\varphi)\,\mathrm{d}\varphi \\ &\quad + \frac{1}{2\,\pi}\int_{-\pi}^{\pi}\left[\sum_{j=0}^{M-1} p_k(2\,\pi\,\rho\,j+\varphi)\right]^2 \mathrm{d}\varphi \,. \end{aligned} \tag{43}$$

We have thus an expression for the second raw moment which can be combined with the expression for the average of the number of counts of the cumulative histogram, to obtain the variance,

$$\sigma^2_{h_k} = m_{2h_k} - \mu^2_{h_k} \,. \tag{44}$$

Inserting thus (34) and (43) into (44) leads to

$$\begin{aligned} \sigma^2_{h_k} &= \frac{M}{2\,\pi}\int_{-\pi}^{\pi} p_k(\varphi)\,\mathrm{d}\varphi - \frac{M}{2\,\pi}\int_{-\pi}^{\pi} p_k^2(\varphi)\,\mathrm{d}\varphi \\ &\quad + \frac{1}{2\,\pi}\int_{-\pi}^{\pi}\left[\sum_{j=0}^{M-1} p_k(2\,\pi\,\rho\,j+\varphi)\right]^2 \mathrm{d}\varphi \\ &\quad - \left[\frac{M}{2\,\pi}\int_{-\pi}^{\pi} p_k(\varphi)\,\mathrm{d}\varphi\right]^2 . \end{aligned} \tag{45}$$

These four terms can be regrouped into two new terms,

$$\sigma^2_{h_k} = \mu_{\sigma^2_{h_k}} + \sigma^2_{\mu_{h_k}} \,, \tag{46}$$

where

$$\mu_{\sigma^2_{h_k}} = \frac{M}{2\,\pi}\int_{-\pi}^{\pi} p_k(\varphi)\,\mathrm{d}\varphi - \frac{M}{2\,\pi}\int_{-\pi}^{\pi} p_k^2(\varphi)\,\mathrm{d}\varphi \tag{47}$$

and

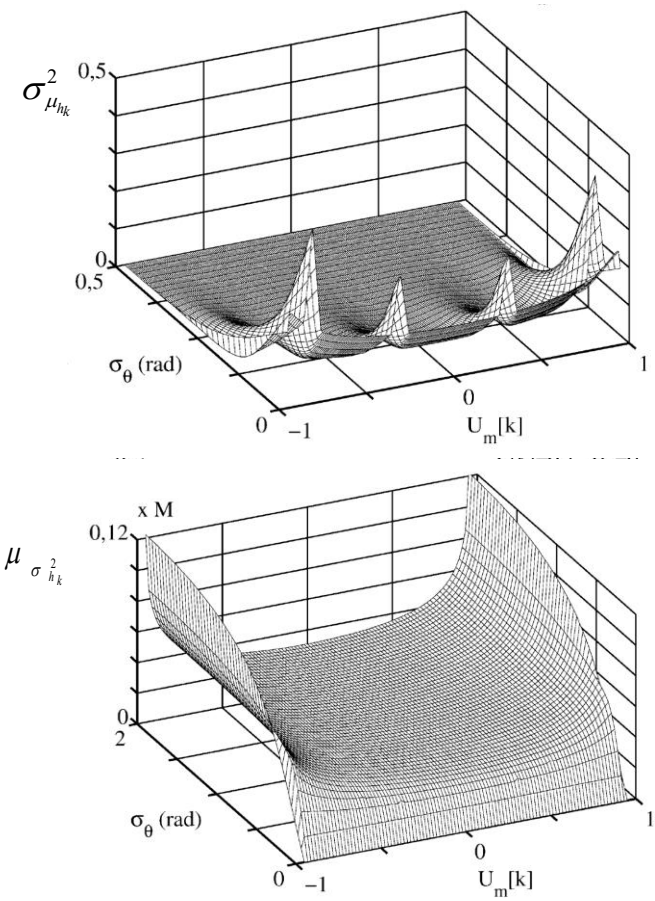

Figure 4. Variance of the conditional mean (top) and mean of the conditional variance (bottom) as a function of transition voltage and phase noise standard deviation for the case of 5 samples.

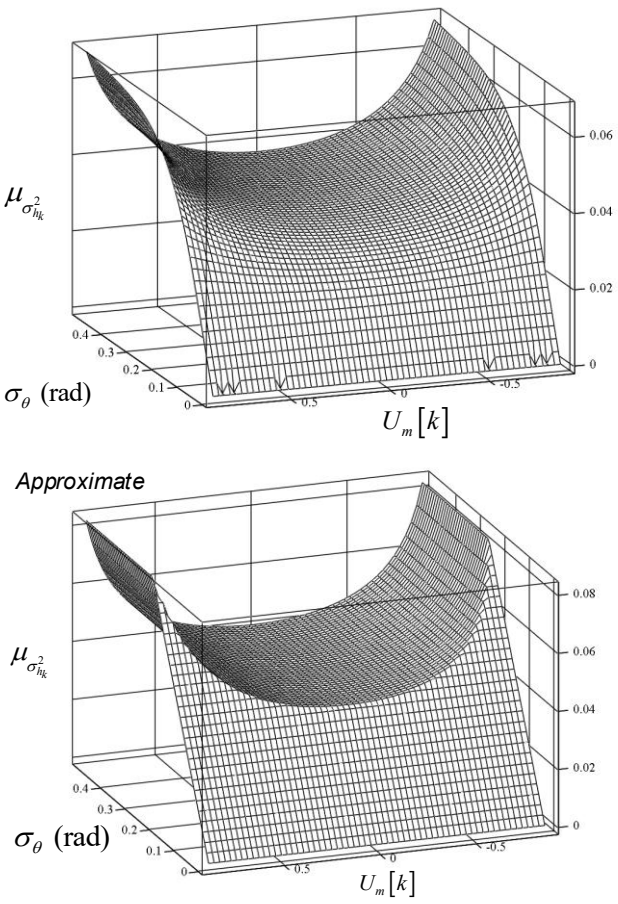

Figure 5. Mean of the conditional variance as a function of transition voltage and phase noise standard deviation for the case of 200 samples. On the top is the actual value and in the bottom is the values given by the mathematical approximation proposed here.

$$\sigma^2_{\mu_{h_k}} = \frac{1}{2\,\pi}\int_{-\pi}^{\pi}\left[\sum_{j=0}^{M-1} p_k(2\,\pi\,\rho\,j+\varphi)\right]^2 \mathrm{d}\varphi - \left[\frac{M}{2\,\pi}\int_{-\pi}^{\pi} p_k(\varphi)\,\mathrm{d}\varphi\right]^2. \quad (48)$$

The two parts into which the variance of the number of histogram counts can be divided are observed separately in Figure 4 as a function of transition voltage and phase noise standard deviation. A small number of samples is used just to illustrate the behaviour of the function. In practice a much larger number is used.

Note that the average of the conditional variance, illustrated in Figure 4, top, and given in (47), is proportional to the number of samples which the variance of the conditional mean, illustrated in Figure 4, bottom, and given by (48), is not. In the latter case only the number of "arcs" along $U_m[k]$ increases with number of samples M. For typical values of the number of samples used, which are at least in the hundreds and can often reach several millions, the second part of the variance of the number of counts of the cumulative histogram, given by (46) is negligible. We can thus assume

$$\sigma^2_{h_k} \approx \mu_{\sigma^2_{h_k|\varphi}} = \frac{M}{2\,\pi}\left[\int_{-\pi}^{\pi} p_k(\varphi)\,\mathrm{d}\varphi - \int_{-\pi}^{\pi} p_k^2(\varphi)\,\mathrm{d}\varphi\right]. \quad (49)$$

We represent this term in Figure 5.

The end goal of this study is to propose a numerical expression for the variance of the estimated DNL that is easy to use. We start that by first proposing one for the variance of the number of counts of the histogram by observing the top image in Figure 5 and making some simplifications. This expression, heuristically derived, is

$$\sigma^2_{h_k} \approx M \cdot \min\left(\frac{Q}{\sqrt{A^2 - T_k^2}}, \frac{2}{\pi\sqrt{\pi}}\sigma_\theta\right), \quad k = 1, 2, \ldots, 2^{n_b} - 1\,. \quad (50)$$

It was obtained by combining two different expressions: one for the observed u-shape in the case of larger phase noise standard deviation values which does not depend on this value, and another for the smaller values of phase noise standard deviation that increases linearly with this value of standard deviation. The value given by this expression is depicted in the bottom of Figure 5. The difference between the actual values and the approximate ones are depicted in Figure 6. With eq. (50) in hand we can now propose a similar expression for the estimated code bin widths.

4. VARIANCE OF THE DIFFERENTIAL NON-LINEARITY ESTIMATION

Here we address the computation of the variance of the code bin widths. This follows closely the author's PhD dissertation

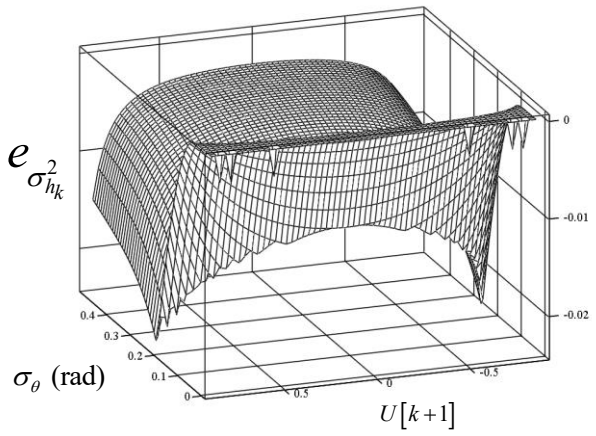

Figure 6. Error of the approximation used for the mean of the conditional variance as a function of transition voltage and phase noise standard deviation for the case of 200 samples.

[28], section 4.2.5. In the next chapter we will finally arrive at the variance of the estimated DNL.

The code bin widths of the ADC under test are obtained from the transition voltages, through (2), which, in turn, are estimated from the number of counts in the cumulative histogram using (1). Combining these two expressions leads us to

$$\widehat{W}_k = A \cdot \cos\left(\pi \frac{c_{k-1}}{M}\right) - A \cdot \cos\left(\pi \frac{c_k}{M}\right), \quad k = 1, 2, \ldots, 2^{n_b} - 2 \tag{51}$$

To compute the variance of this estimated value one should look at it as a function of two random variables, c_{k-1} and c_k. Using the expression in [31], page 156, we can write

$$\sigma^2_{\widehat{W}_k} \approx \left(\frac{\partial \widehat{W}_k}{\partial c_k}\right)^2 \cdot \sigma^2_{c_k} + 2 \cdot \frac{\partial \widehat{W}_k}{\partial c_k} \cdot \frac{\partial \widehat{W}_k}{\partial c_{k-1}} \cdot r \cdot \sigma_{c_k} \cdot \sigma_{c_{k-1}} + \left(\frac{\partial \widehat{W}_k}{\partial c_{k-1}}\right)^2 \cdot \sigma^2_{c_{k-1}}, \tag{52}$$

where r is the correlation coefficient of the variables c_k and c_{k-1}. The partial derivatives are to be taken at $c_k = \mu_{c_k}$ and $c_{k-1} = \mu_{c_{k-1}}$. Using (51) leads to

$$\sigma^2_{\widehat{W}_k} \approx \left[\frac{A\,\pi}{M} \sin\left(\pi \frac{\mu_{c_k}}{M}\right)\right]^2 \cdot \sigma^2_{c_k} + 2 \cdot \left[\frac{A\,\pi}{M} \sin\left(\pi \frac{\mu_{c_k}}{M}\right)\right] \cdot \left[\frac{A\,\pi}{M} \sin\left(\pi \frac{\mu_{c_{k-1}}}{M}\right)\right] \cdot r \cdot \sigma_{c_k} \cdot \sigma_{c_{k-1}} + \left[\frac{A\,\pi}{M} \sin\left(\pi \frac{\mu_{c_{k-1}}}{M}\right)\right]^2 \cdot \sigma^2_{c_{k-1}} \tag{53}$$

Considering now the limit where the code bin length goes to 0 one has $\mu_{c_k} \approx \mu_{c_{k-1}}$. We can thus simplify this expression to

$$\lim_{W_k \to 0} \sigma^2_{\widehat{W}_k} \approx \left(\frac{A\,\pi}{M}\right)^2 \cdot \sin^2\left(\pi \frac{\mu_{c_{k-1}}}{M}\right) \cdot \left(\sigma^2_{c_k} + 2r \cdot \sigma_{c_k} \cdot \sigma_{c_{k-1}} + \sigma^2_{c_{k-1}}\right). \tag{54}$$

Since

$$h_k = c_k - c_{k-1}, k = 1, 2, \ldots, 2^{n_b} - 2, \tag{55}$$

we can replace the last parenthesis in (54) by $\sigma^2_{h_k}$. As such one gets

$$\lim_{W_k \to 0} \sigma^2_{\widehat{W}_k} \approx \left(\frac{A\,\pi}{M}\right)^2 \cdot \sin^2\left(\pi \frac{\mu_{c_{k-1}}}{M}\right) \cdot \sigma^2_{h_k}. \tag{56}$$

Considering that the presence of phase noise does not affect the mean value of the number of counts of the cumulative histogram. One can thus write

$$\lim_{W_k \to 0} \sigma^2_{\widehat{W}_k} \approx \left(\frac{A\,\pi}{M}\right)^2 \cdot (1 - U_k^2) \cdot \sigma^2_{h_k}. \tag{57}$$

Finally, considering that the DNL estimation is given by (6), with a unit gain, we have

$$\lim_{W_k \to 0} \sigma^2_{\widehat{DNL}_k} \approx \left(\frac{A\pi}{M \cdot Q}\right)^2 \cdot (1 - U_k^2) \cdot \sigma^2_{h_k} \tag{58}$$

Inserting (50) leads to

$$\lim_{W_k \to 0} \sigma^2_{\widehat{DNL}_k} \approx \frac{\pi^2}{M} \cdot \frac{A^2 - T_k^2}{Q^2} \cdot \min\left(\frac{Q}{\sqrt{A^2 - T_k^2}}, \frac{2}{\pi\sqrt{\pi}}\sigma_\theta\right), \quad k = 1, 2, \ldots, 2^{n_b} - 1. \tag{59}$$

This is the final expression proposed in this work. It allows one to compute the minimum number of samples to use in order to achieve a certain bound on the precision of the DNL estimation, given the amount of phase noise present. This result also has value a-posteriori, after the ADC test has been carried out, to compute the precision of the result given the test conditions.

Furthermore, since the precision of the DNL estimation depends on the position of the output code on the transfer function, through $A^2 - T_k^2$, we may chose the amount of overvoltage to use to make sure that the code widths, and DNL values, in the edges of the transfer function, are estimated with sufficient precision by using a proper amount of overdrive. Recall that overdrive means to use an amplitude of the sinusoidal stimulus signal that is larger than the ADC full scale range in order to guarantee that, in the event of poor accuracy from the function generator or gain error in the ADC, all codes are excited.

It is straightforward to write equation (59) in such a way as to give the minimum number of samples required to achieve a given bound, B_{DNL}, on the precision of the estimated DNL values:

$$M \geq \frac{\pi^2}{B_{\mathrm{DNL}}} \cdot \frac{A^2 - T_{\max}^2}{Q^2} \cdot \max\left(\frac{Q}{\sqrt{A^2 - T_{\max}^2}}, \frac{2}{\pi\sqrt{\pi}}\sigma_\theta\right), \tag{60}$$

where a bipolar ADC was considered where the first and last transition voltages are symmetric with a value $T_{\max}$. It is common to use a parameter called overdrive which represents the relative amount that the stimulus signal amplitude is greater that the higher (in absolute value) transition voltage:

$$\alpha = \frac{A}{T_{\max}}. \tag{61}$$

Replacing A by $\alpha \cdot T_{\max}$ in (60) leads to

$$M \geq \frac{\pi^2}{B_{\mathrm{DNL}}} \cdot (\alpha^2 - 1)\left(\frac{T_{\max}}{Q}\right)^2 . \max\left(\frac{Q}{T_{\max}} \cdot \frac{1}{\sqrt{\alpha^2 - 1}}, \frac{2}{\pi\sqrt{\pi}}\sigma_\theta\right). \quad (62)$$

Using

$$\frac{T_{\max}}{Q} \approx 2^{n_b - 1}, \quad (63)$$

we can also write, for the minimum number of samples to use,

$$MM \geq \frac{\pi^2}{B_{\mathrm{DNL}}} \cdot (\alpha^2 - 1) \cdot 2^{(2n_b - 2)} \cdot \max\left(\frac{1}{2^{n_b - 1}} \cdot \frac{1}{\sqrt{\alpha^2 - 1}}, \frac{2}{\pi\sqrt{\pi}}\sigma_\theta\right), \quad (64)$$

which give us the minimum number of samples to use as a function of the bound on the DNL estimation precision, the number of ADC bits, the phase noise standard deviation and the amount of overdrive desired which ranges typically from 5% to10%.

5. MONTE CARLO VALIDATION

In order to validate the analytical expression proposed here to determine the precision of the DNL estimations obtained with the code density test of ADC, a Monte Carlo type set of numerical simulations were carried out. The results are presented in Figure 7. A simulated ADC test was repeated 2000 times with the code density test using 200 samples in each run. The stimulus signal used was a sinewave with an amplitude equal to the ADC full scale and a frequency related to the sampling frequency such that the samples simulated covered exactly one period. The ADC simulated had 4 bits and a Full Scale range of ±1 V. The phase noise created was normally distributed with a standard deviation from 0 to 0.3 rad.

The result of this simulations show that the analytical expression presented guarantee an upper bound for the DNL standard deviation estimated (vertical error bars). In the top chart we see the precision for the DNL value of quantization level in the case of two values of phase noise standard deviation: 0.05 rad and 0.3 rad.

In the chart on the bottom of Figure 7, we observe the results as a function of phase noise standard deviation for two specific transfer function levels: the first one and the middle one. The range of values of phase noise standard deviation simulated is rather large. In practical conditions it is common to encounter an amount of phase noise with a standard deviation lower than0.05 rad. For those data points the error bars are around the theoretical values depicted with the solid lines.

6. CONCLUSIONS

A mathematical derivation was presented which addresses the problem of estimating the precision of the differential nonlinearity (DNL) of an analogue to digital converter (ADC) estimated using the code density test. The result was a new analytical expression proposed here that related the standard deviation of the DNL estimates with the test parameters,

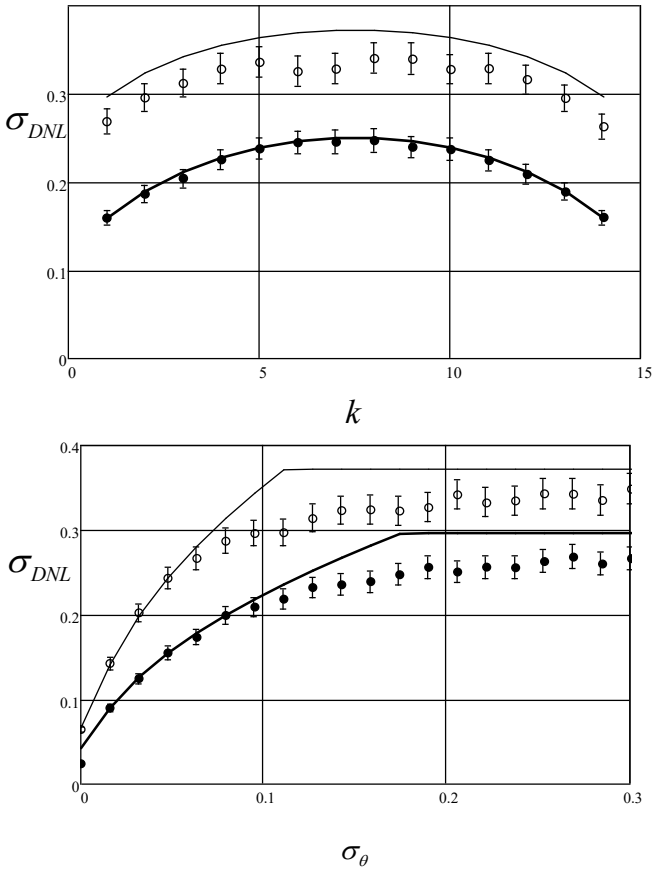

Figure 7. Results of the Monte Carlo validation. On the top we have the mean of the conditional variance as a function of the code bin index for two phase noise standard deviation values: 0.05 rad (thick) and 0.3 rad (thin). On the bottom we have the same variance as a function of phase noise standard deviation for two output codes: the first one, k = 0, with the thick trace and the middle one, k = 8 with the thin trace. Both figures are for a 4-bit ADC with a full-scale range of 1 V. The stimulus signal is sinusoidal with an amplitude of 1.05 V (5% overvoltage) The number of samples acquired is 200 and the number of test repetitions carried for the Monte Carlo simulation (circles and error bars) is 2000.

namely, the number of samples used, the standard deviation of the phase noise present, the sinusoidal stimulus signal amplitude, the ADC transition voltage values and ideal code bin width.

The correctness of this expression was validated using a Monte Carlo type numerical simulation. Two principles guided the derivation of the mathematical equation obtained in the end: the accuracy of the values given by it compared with the actual values of DNL and the ease of use by an engineer. In particular, one wanted to have an expression that could be use, before a given test is carried out, to help choose, for example, the number of samples (M) that should be acquired given a bound on the DNL standard deviation. It was thus fundamental that the expression could be easily rearranged to give the number of samples as a function of the phase noise standard deviation and bound on the DNL estimation standard deviation. That was presented in equation (64).

In conclusion, the content of this work is believed to be useful to an engineer testing ADCs using the code density test method.

REFERENCES

[1] R. E. Wilkes, J. J. Tobin, Digital Telephony and Network Integration, Artech House Publishers, 2003.

[2] F. Lamb, Industrial Automation: Hands-On, McGraw-Hill Education, 2013.

[3] E. Gertz, P. Di Justo, Environmental Monitoring with Arduino: Building Simple Devices to Collect Data About the World Around Us, Maker Media, Inc., 2012.

[4] N. Zaman, Automotive Electronics Design Fundamentals, CRC Press, 2020.
DOI: 10.1007/978-3-319-17584-3

[5] P. Pandian, G. Uma, M. Umapathy, Design and Simulation of MEMS Electrothermal Compliant Actuator-Based Analog-to-Digital Converter, Arabian Journal for Science and Engineering, pp. 1823-1831, February 2018.

[6] W. Kester, Data Conversion Handbook, Analog Devices, 2004.

[7] IEEE Standard 1057-2017, IEEE Standard for Digitizing Waveform Recorders, IEEE 2017.
DOI: 10.1109/IEEESTD.2018.8291741

[8] IEEE Standard 1241-2010, IEEE Standard for Terminology and Test Methods for Analog-to-Digital Converters, IEEE, 2010.
DOI: 10.1109/IEEESTD.2011.5692956

[9] R. Holcer, L. Michaeli, J. Saliga, DNL ADC testing by the exponential shaped voltage, IEEE Transactions on Instrumentation and Measurement, vol. 52, no. 3, June 2003, pp. 946-949.
DOI: 10.1109/TIM.2003.814668

[10] D. R. White, C. P. Pickup, Systematic errors in digital cross correlators due to quantization and differential nonlinearity, in IEEE Transactions on Instrumentation and Measurement, vol. IM-36, no. 1, March 1987, pp. 47-53.
DOI: 10.1109/TIM.1987.6312629

[11] J. Blair, Histogram measurement of ADC nonlinearities using sine waves, IEEE Transactions on Instrumentation and Measurement, vol. 43, no. 3, June 1994, pp. 373-383.
DOI: 10.1109/19.293454

[12] F. Stefani, D. Macii, A. Moschitta, P. Carbone, D. Petri, Simple and time-effective procedure for ADC INL estimation, IEEE Transactions on Instrumentation and Measurement, vol. 55, no. 4, Aug. 2006, pp. 1383-1389.
DOI: 10.1109/TIM.2006.876395

[13] S. C. Vora, L. Satish, ADC Static Nonlinearity Estimation Using Linearity Property of Sinewave, IEEE Transactions on Instrumentation and Measurement, vol. 60, no. 4, April 2011, pp. 1283-1290.
DOI: 10.1109/TIM.2010.2084773

[14] F. Corrêa Alegria, A. Cruz Serra, Standard Histogram Test Precision of ADC Gain and Offset Error Estimation, IEEE Transactions on Instrumentation and Measurement, vol. 56, no. 5, Oct. 2007, pp. 1527-1531.
DOI: 10.1109/TIM.2007.907978

[15] P. Carbone, D. Petri, Noise sensitivity of the ADC histogram test, IEEE Transactions on Instrumentation and Measurement, vol. 47, no. 4, Aug. 1998, pp. 1001-1004.
DOI: 10.1109/19.744658

[16] F. Corrêa Alegria, A. Cruz Serra, Influence of Frequency Errors in the Variance of the Cumulative Histogram in ADC Testing, IEEE Transactions in Instrumentation and Measurement, vol. 50, no. 2, 2001, pp. 161-164.
DOI: 10.1109/19.918166

[17] M. Löhning, G. Fettweis, The effects of aperture jitter and clock jitter in wideband ADCs, Computer Standards and Interfaces, vol. 29, no. 1, 2007, pp. 11-18.
DOI: 10.1016/j.csi.2005.12.005

[18] E. Rubiola, Phase Noise and Frequency Stability in Oscillators, Cambridge University Press, 2009.

[19] L. Springer, F. Ludwig, U. Mavrič, (+ another 6 authors), Phase Noise Measurements for L-Band Applications at Attosecond Resolution, IEEE Transactions on Instrumentation and Measurement, vol. 71, 2022, Art no. 8003307, pp. 1-7.
DOI: 10.1109/TIM.2022.3170975

[20] F. Corrêa Alegria, A. Cruz Serra, Gaussian Jitter Induced Bias of Sine Wave Amplitude Estimation Using Three-Parameter Sine Fitting, IEEE Transactions on Instrumentation and Measurement, vol. 59, no. 9, Sept. 2010, pp. 2328-2333.
DOI: 10.1109/TIM.2009.2034576

[21] F. Corrêa Alegria, Precision of Harmonic Amplitude Estimation on Jitter Corrupted Data Using Sine Fitting, Signal Processing, Elsevier, vol. 92, no. 3, March 2012, pp. 807-818.
DOI: 10.1016/j.sigpro.2011.09.027

[22] F. Corrêa Alegria, A. M. da Cruz Serra, Overdrive in the ramp histogram test of ADCs, IEEE Transactions on Instrumentation and Measurement, vol. 54, no. 6, Dec. 2005, pp. 2305-2309.
DOI: 10.1109/TIM.2005.858549

[23] L. Jin, D. Chen, R. L. Geiger, Code-Density Test of Analog-to-Digital Converters Using Single Low-Linearity Stimulus Signal, IEEE Transactions on Instrumentation and Measurement, vol. 58, no. 8, Aug. 2009, pp. 2679-2685.
DOI: 10.1109/TIM.2009.2015700

[24] S. C. Vora, L. Satish, ADC Static Characterization Using Nonlinear Ramp Signal, IEEE Transactions on Instrumentation and Measurement, vol. 59, no. 8, Aug. 2010, pp. 2115-2122.
DOI: 10.1109/TIM.2009.2031852

[25] F. Corrêa Alegria, P. Arpaia, A. Cruz Serra, P. Daponte, Performance Analysis of an ADC Histogram Test Using Small Triangular Waves, IEEE Transactions in Instrumentation and Measurement, vol. 51, no. 4, 2002, pp. 723-729.
DOI: 10.1109/TIM.2002.803292

[26] F. Corrêa Alegria, A. Cruz Serra, Error in the Estimation of Transition Voltages with the Standard Histogram Test of ADCs, Measurement, vol. 35, no. 4, 2004, pp. 389-397.
DOI: 10.1016/j.measurement.2004.03.003

[27] F. Corrêa Alegria, A. Cruz Serra, The Histogram Test of ADCs With Sinusoidal Stimulus Signal is Unbiased by Phase Noise, IEEE Transactions on Instrumentation and Measurement, vol. 58, no. 11, 2009, pp. 3847-3854.
DOI: 10.1109/TIM.2009.2020842

[28] F. Corrêa Alegria, Caracterização Estática e Dinâmica de Conversores Analógico/Digitais pelo Método do Histograma, PhD Thesis, 2002. [in Portuguese]

[29] F. Corrêa Alegria, Phase Noise Influence on the Transfer Function Estimation of Analog to Digital Converters Using the Histogram Method, IEEE Access, vol. 13, 2025, pp. 32051-32062.
DOI: 10.1109/ACCESS.2025.3541559

[30] F. Corrêa Alegria, A. Cruz Serra, Uncertainty in the ADC Transition Voltages Determined with the Histogram Method, Proc. of the 6th Workshop on ADC Modeling and Testing, Lisbon, Portugal, 13-14 September 2001, pp. 28-32. Online [Accessed 21 June 2025]
https://www.imeko.info/publications/tc4-2001/IMEKO-TC4-2001-091.pdf

[31] A. Papoulis, Probability, Random Variables and Stochastic Processes, McGraw-Hill, 3rd edition, 1991.